Zero and controllable thermal expansion in $HfMgMo_{3-x}W_xO_{12}$*

Tao Li(李涛)[1], Xian-Sheng Liu(刘献省)[2], Yong-Guang Cheng(程永光)[1,3], Xiang-Hong Ge(葛向红)[1], Meng-Di Zhang(张孟迪)[1], Hong Lian(连虹)[1], Ying Zhang(张莹)[1], Er-Jun Liang(梁二军)[1,†], and Yu-Xiao Li(李玉晓)[1,‡]

[1] *School of Physical Science & Engineering and Key Laboratory of Materials Physics of Ministry of Education, Zhengzhou University, Zhengzhou* 450052, *China*

[2] *Henan Key Laboratory of Photovoltaic Materials and School of Physics and Electronics, Henan University, Kaifeng* 475004, *China*

[3] *School of Physical Science & Engineering and Key Laboratory of Materials Physics of Ministry of Education, Zhengzhou University, Zhengzhou* 450052, *China*

(Received 22 July 2016; revised manuscript received 25 October 2016; published online 29 November 2016)

$HfMgMo_{3-x}W_xO_{12}$ with $x = 0.5$, 1.0, 1.5, 2.0, and 2.5 are developed with a simple solid state method. With increasing the content of W, solid solutions of $HfMgMo_{3-x}W_xO_{12}$ crystallize in an orthorhombic structure for $x \leq 2.0$ and a monoclinic structure for $x > 2.0$. A near-zero thermal expansion (ZTE) is realized for $HfMgMo_{2.5}W_{0.5}O_{12}$ and negative coefficients of thermal expansion (NCTE) are achieved for other compositions with different values. The ZTE and variation of NCTE are attributed to the difference in electronegativity between W and Mo and incorporation of a different amount of W, which cause variable distortion of the octahedra and softening of the MoO_4 tetrahedra, and hence an enhanced NCTE in the *a*- and *c*-axis and reduced CTE in the *b*-axis as revealed by Raman spectroscopy and x-ray diffraction.

Keywords: zero thermal expansion, negative thermal expansion, orthorhombic structure, solid solution, Raman spectroscopy

PACS: 65.40.De, 81.05.Je, 61.50.–f, 78.30.–j **DOI:** 10.1088/1674-1056/26/1/016501

1. Introduction

Negative thermal expansion (NTE) materials are becoming very attractive due to their potential applications in tailoring the coefficient of thermal expansion (CTE) to reduce thermal stress.[1–12] To date, different families of NTE materials based on various mechanisms, such as the phonon effect,[2,13–16] magnetovolume effect,[5] spontaneous ferroelectric polarization,[4] and charge transfer,[17,18] have been reported.

Of the NTE materials, the $A_2M_3O_{12}$ (A = Fe, Al, Cr, Y, Yb, Er, etc. M = Mo, W) family has received considerable interests due to its chemical flexibility and hence tailorable NTE. A modified structure of ABM_3O_{12} was also possible to present the NTE property. $HfMgW_3O_{12}$ was first reported by Suzuki and Omote in 2004[19] and identified as an orthorhombic structure with space group *Pnma* at room temperature (RT) and above.[19] Nevertheless, Gindhart and Lind[20] through variable temperature neutron and x-ray diffraction characterization showed that $HfMgW_3O_{12}$ was crystallized in monoclinic structure with space group $P2_1/a$ below 400 K and was transformed to an orthorhombic structure with space group *Pnma* at higher temperatures. Its linear CTE is -1.2×10^{-6} K^{-1} in the orthorhombic phase. $HfMgMo_3O_{12}$ with a low linear CTE of 1.02×10^{-6} K^{-1} from 298 to 1013 K was reported by Marinkovic *et al.* in 2008.[21] It crystallizes in orthorhombic symmetry with space group *Pnma*(62) or *Pna*21 (33)[21] and transforms to monoclinic structure at 175 K.[22] Baiz *et al.*[23] reported non-hydrolytic sol-gel synthesis of $HfMgW_3O_{12}$ and $ZrMgW_3O_{12}$ without referring to the structure and property. $ZrMgMo_3O_{12}$ was shown to be an orthorhombic structure without phase transition from 113 K to 1200 K and the linear CTE is about -3.8×10^{-6} K^{-1} (300–1000 K),[24] while $ZrMgW_3O_{12}$ was reported to be highly hygroscopic, and its linear CTE is -1.15×10^{-6} K^{-1} (440–975 K) after releasing crystal water.[25]

As mentioned above, $HfMgMo_3O_{12}$ and $HfMgW_3O_{12}$ have a low positive and NTE, respectively. In the paper, we report the synthesis and thermal expansion properties of the solid solutions of $HfMgMo_{3-x}W_xO_{12}$ with $x = 0.5$, 1.0, 1.5, 2.0, and 2.5 to achieve zero and controllable thermal expansion without hygroscopicity.

2. Experimental details

Analytical grade reagents of HfO_2, MgO, WO_3, MoO_3 were used as raw materials, which were weighted and ground according to the molar ratios of the destination materials $HfMgMo_{3-x}W_xO_{12}$ with $x = 0.5$, 1.0, 1.5, 2.0, and 2.5. The mixed raw materials were pressed into cylinders using a uni-

*Project supported by the National Natural Science Foundation of China (Grant Nos. 10974183 and 11104252), the Key Natural Science Project of Henan Province, China (Grant No. 142102210073), the Doctoral Fund of the Ministry of Education of China (Grant No. 20114101110003), and the Fund for Science & Technology Innovation Team of Zhengzhou, China (Grant No. 112PCXTD337).

†Corresponding author. E-mail: ejliang@zzu.edu.cn

‡Corresponding author. E-mail: liyuxiao@zzu.edu.cn

© 2017 Chinese Physical Society and IOP Publishing Ltd

axis tablet machine with pressure about 200 MPa. The pressed pellets were sintered at 1073–1323 K for 3 h in a muffle furnace in air. For comparison, $HfMgMo_3O_{12}$ and $HfMgW_3O_{12}$ were also prepared.

X-ray diffraction (XRD) measurements were carried out with an x-ray diffractometer (Model X'Pert PRO) to identify the crystalline phase. Raman spectra were recorded with a Jobin-Yvon LabRAM HR Evolution Raman spectrometer equipped with a TMS 94 heating/freezing stage (an accuracy of ±0.1 K). A laser excitation wavelength of 633 nm was used. The differential scanning calorimetry (DSC) measurements were carried out on a Netzsch STA 449F3 simultaneous thermal analyzer in the temperature range of 293–1073 K with the heating rates of 10 K/min. The microstructures and energy dispersive spectra of the samples were examined with a scanning electron microscope (SEM, Model Quanta 250). The linear CTEs were measured with a dilatometer (Linseis DIL L76).

3. Results and discussion

3.1. Crystal structure analysis

Figure 1 shows the XRD patterns of $HfMgMo_{3-x}W_xO_{12}$ with $x = 0.5$, 1.0, 1.5, 2.0, and 2.5 at RT. It was reported that $HfMgMo_3O_{12}$ crystallizes in an orthorhombic structure with space group *Pnma*.[21] There are not obvious changes in the XRD patterns with increasing the content of W. This is probably the reason that $HfMgW_3O_{12}$ was identified as an orthorhombic structure with space group *Pnma*[19] or a monoclinic structure with space group $P2_1/a$ below 400 K[20] by different groups.

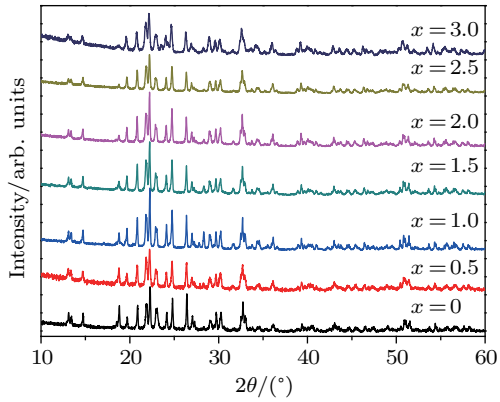


Fig. 1. (color online) XRD patterns of $HfMgMo_{3-x}W_xO_{12}$ with $x = 0.5$, 1.0, 1.5, 2.0, and 2.5. For comparison, the XRD patterns of $HfMgMo_3O_{12}$ and $HfMgW_3O_{12}$ are also presented.

In Fig. 2 we show Raman spectra of $HfMgMo_{3-x}W_xO_{12}$ with $x = 0$, 0.5, 1.0, 1.5, 2.0, 2.5, and 3 for the external librational and translational vibrations of the polyhedra (a) and internal symmetric stretching vibrations of the MoO_4/WO_4 tetrahedra (b), respectively. Figure 2(a) indicates that the Raman spectra for $x \leq 2.0$ have similar features in the low wave number region while those for $x > 2.0$ are different as indicated by the disappearance of the Raman modes between 60 and 120 cm^{-1}. The insert shows the temperature-dependent Raman spectra of $HfMgW_3O_{12}$. It is obvious that a Raman mode at about 92 cm^{-1} appears at 423 K and exhibits a redshift with increasing temperature. Besides, a Raman mode at about 33 cm^{-1} at RT shifts to blue with increasing temperature till 373 K, and a Raman mode at about 38 cm^{-1} appears at 423 K which shifts a little with increasing temperature. The low wavenumber external librational and translation vibrations are the origins for NTE. These results suggest strongly that (i) $HfMgW_3O_{12}$ adopts a monoclinic structure at RT and transforms to an orthorhombic one above 400 K; (ii) $HfMgMo_{3-x}W_xO_{12}$ adopts an orthorhombic phase for $x \leq 2.0$ and a monoclinic structure for $x > 2.0$.

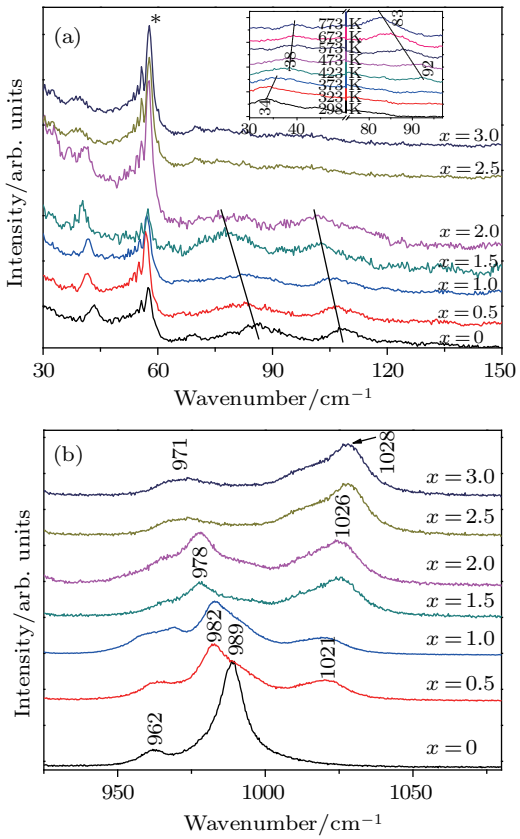


Fig. 2. (color online) Raman spectra of $HfMgMo_{3-x}W_xO_{12}$ with $x = 0$, 0.5, 1.0, 1.5, 2.0, 2.5, and 3 for the low wavenumber (a) and high wavenumber (b) regions, respectively. The insert shows the temperature-dependent Raman spectra of $HfMgW_3O_{12}$. The sharp peak denoted by an asterisk (*) is the sparkle from air plasma.

The most distinct change of the Raman spectra in the symmetric stretching region is the appearance of the Raman band at about 1021 cm^{-1} for $x = 0.5$ which increases in intensity and shifts progressively to 1028 cm^{-1} with increasing the contents of W. This band can be assigned unambiguously to the W = O symmetric stretching vibrations. The blue shift indicates a hardening of the WO_4 tetrahedra with increasing the

contents of W. Another distinct change is the obvious red shift of the Mo = O symmetric stretching band at about 990 cm^{-1} for $HfMgMo_3O_{12}$ which shifts to 983 cm^{-1} for $x = 0.5$ and to 978 cm^{-1} for $x = 1.5$, indicating a progressive weakening of MoO_4 tetrahedra with increasing the contents of W. In the orthorhombic structure, each HfO_6/MgO_6 octahedron shares its corners with six MoO_4/WO_4 tetrahedra and each MoO_4/WO_4 tetrahedron shares its corners with four HfO_6/MgO_6 octahedra. Since the electronegativity of W (2.36) is larger than that of Mo (2.16), it has a higher ability to attract electrons to the W = O bond, leading to weakening of the Mo = O bond if they share the same HfO_6/MgO_6 octahedron. Due to the difference in electronegativity and cation radius between W and Mo, a distortion for the octahedra is expected.

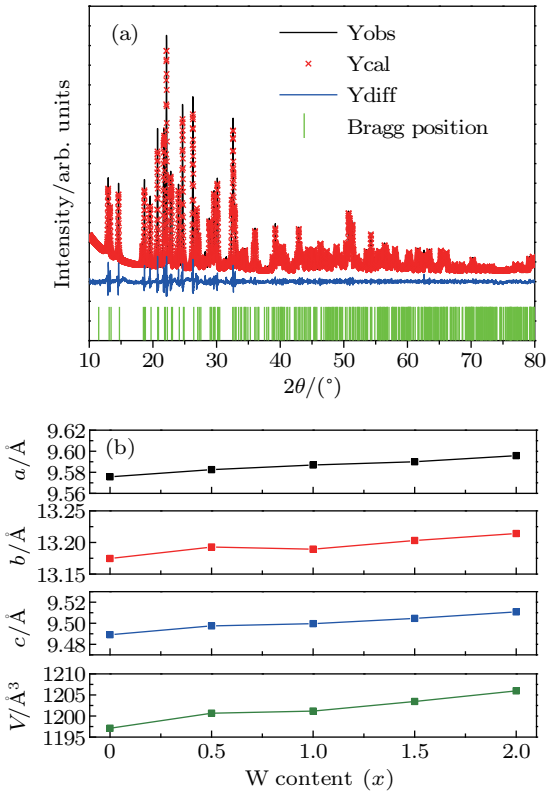


Fig. 3. (color online) (a) Structure refinement by the Pawley method with space group *Pnma*. Tick marks (bottom) indicate positions of the $HfMgMo_{2.5}W_{0.5}O_{12}$ diffraction lines and the curve in the middle is the difference between the experimental and fitted results. (b) Lattice constants and volume change of $HfMgMo_{3-x}W_xO_{12}$ with $x = 0.5$, 1.0, 1.5, and 2.0.

To confirm the crystal structure, structure analysis was performed by the Pawley refinement of XRD patterns with the Academic software of TOPAS 4.0. Figure 3(a) shows the results for $HfMgMo_{2.5}W_{0.5}O_{12}$. It is shown that $HfMgMo_{2.5}W_{0.5}O_{12}$ adopts an orthorhombic structure with space group *Pnma* (62), with acceptable values of $R_{exp} = 5.09\%$, $R_{wp} = 7.02\%$, and $R_p = 5.26\%$. The obtained lattice constants for the *a*-, *b*-, and *c*-axes at RT are $a = 9.5781$ Å, $b = 13.1801$ Å, and $c = 9.4927$ Å, respectively. The samples for $x = 1.0$, 1.5, 2.0, and 2.5 are analyzed with the same method. It is shown that structure for $x = 1.0$, 1.5, 2.0 can be better refined with space group *Pnma* (orthorhombic) while that for $x = 2.5$ can be better refined with space group $P2_1/a$ (monoclinic). For example, the obtained *R*-values for $x = 2.0$ are $R_{exp} = 4.80$, $R_{wp} = 9.30$, and $R_p = 7.21$ with space group *Pnma* and $R_{exp} = 4.76$, $R_{wp} = 14.42$ and $R_p = 10.59$ with space group $P2_1/a$. The results confirm our Raman analysis above. Figure 3(b) shows the lattice constants and volume for $x \leq 2.0$. It is evident that the lattice constants increase with the contents of W but with different ratios in different directions. For example, with respect to $HfMgMo_3O_{12}$, the lattice constants of $HfMgMo_{2.5}W_{0.5}O_{12}$ and $HfMgMo_{1.5}W_{1.5}O_{12}$ are increased by 0.077%, 0.175%, and 0.104% and by 0.182%, 0.375%, and 0.232% for the *a*-, *b*-, and *c*-axes, respectively. It is possibly a result of the distortion of the octahedra and bond angle changes caused by partial substitution of W for Mo.

3.2. Micro morphology of $HfMgMo_{3-x}W_xO_{12}$

Figure 4(a) shows the SEM images ((a1)–(a7)) of $HfMgMo_{3-x}W_xO_{12}$ with $x = 0$, 0.5, 1.0, 1.5, 2.0, 2.5, and 3. For the samples with $x = 0$ and 0.5, the grain morphology presents a spherical shape about 1 μm. With increasing the content of W from 1.0 to 2.0, the average grain sizes increase to near 3 μm with unobvious porosity. Especially, when the content of W increases to 2.5 and 3, the grain morphology transforms from sphere to rod. Figure 4(b) presents the EDS spectra ((b1)–(b7)) of $HfMgMo_{3-x}W_xO_{12}$ with $x = 0$, 0.5, 1.0, 1.5, 2.0, 2.5, and 3. When the content of W increases to 2.5 and 3, i.e., the content of W is larger than that of 2Mo, the relative intensity of the spectra present notable change: the intensity of W is higher than that of Hf, which corresponds to the formation of rod morphology grains.

3.3. Thermal expansion property

The relative length changes of $HfMgMo_{3-x}W_xO_{12}$ with $x = 0.5$, 1.0, 1.5, 2.0, and 2.5 were measured with a dilatometer (Fig. 5). It is found that all the samples of $HfMgMo_{3-x}W_xO_{12}$ with $x = 0.5$, 1.0, 1.5, 2.0, and 2.5 present low CTE or NTE property. Especially, the sample of $HfMgMo_{2.5}W_{0.5}O_{12}$ presents near-zero thermal expansion (ZTE) with $\alpha = 0.48 \times 10^{-6}$ K^{-1}. The largest NTE is observed for $HfMgMo_{1.5}W_{1.5}O_{12}$ which is about -3.91×10^{-6} K^{-1}.

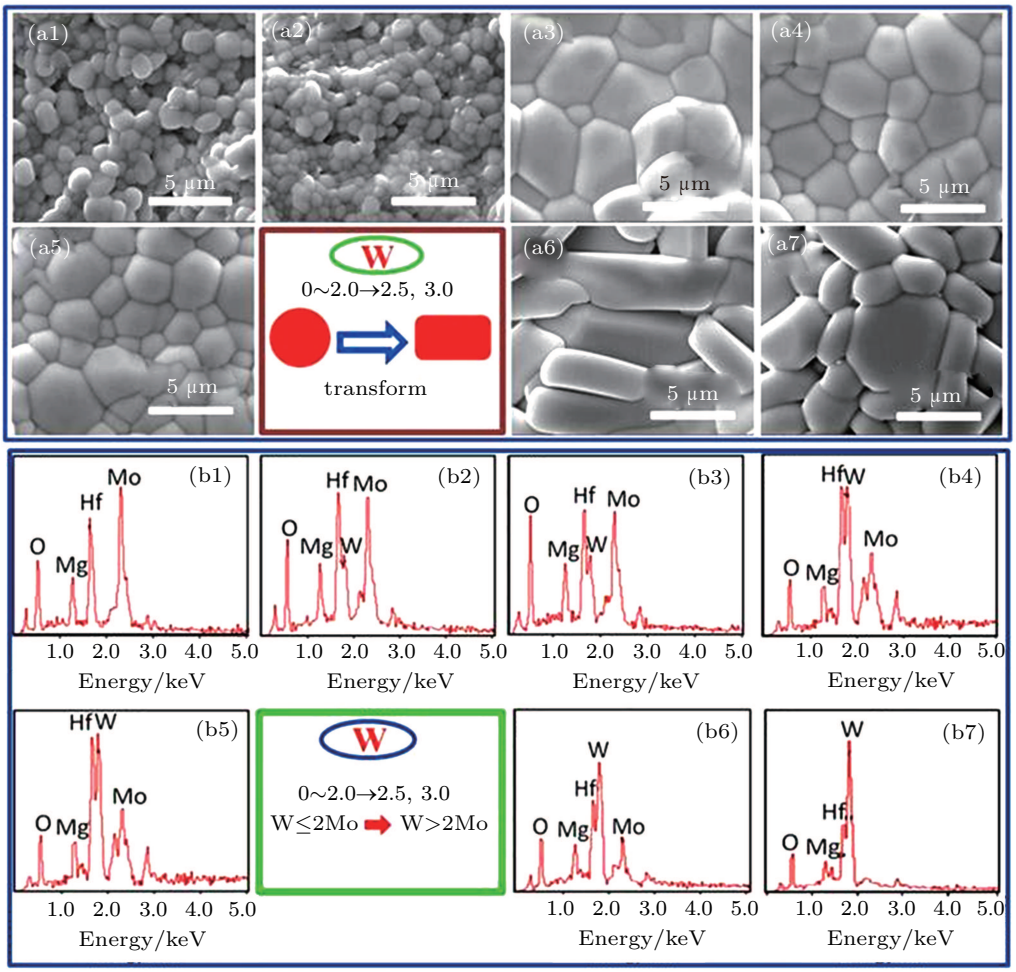


Fig. 4. (color online) SEM images (a) and EDS spectra (b) of $HfMgMo_{3-x}W_xO_{12}$ with $x = 0.5$, 1.0, 1.5, 2.0, and 2.5. For comparison, SEM images (a) and EDS spectra (b) of $HfMgMo_3O_{12}$ and $HfMgW_3O_{12}$ are also presented.

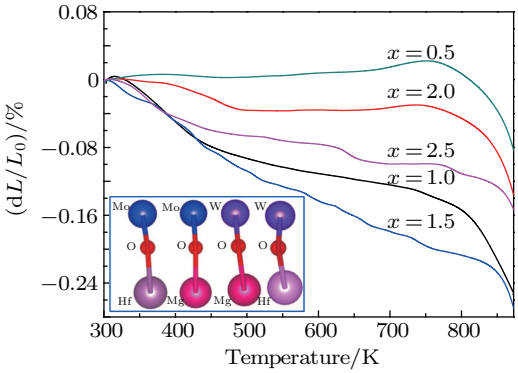


Fig. 5. (color online) Relative length changes of $HfMgMo_{3-x}W_xO_{12}$ with $x = 0.5$, 1.0, 1.5, 2.0, and 2.5.

In order to see whether the ZTE for $HfMgMo_{2.5}W_{0.5}O_{12}$ is intrinsic or not, we measured the XRD of the samples at different temperatures and calculated axial and volume parameters at each temperature. Figure 6(a) shows the selected temperature-dependent XRD patterns for $HfMgMo_{2.5}W_{0.5}O_{12}$. Figure 6(b) shows the changes of the lattice constants and volume with temperature. It is evident that the *a*- and *c*-axes contract while the *b*-axis expands with increasing temperature, giving rise to near-ZTE in volume. The CTEs for the *a*-, *b*-, and *c*-axes and volume are calculated to be $\alpha_a = -5.13 \times 10^{-6}$ K^{-1}, $\alpha_b = 8.15 \times 10^{-6}$ K^{-1}, $\alpha_c = -3.23 \times 10^{-6}$ K^{-1}, $\alpha_v = -2.29 \times 10^{-7}$ K^{-1}, respectively. This gives rise to a linear CTE $\alpha_l = -0.76 \times 10^{-7}$ K^{-1}, confirming that $HfMgMo_{2.5}W_{0.5}O_{12}$ is intrinsically a ZTE material. Compared to $HfMgMo_3O_{12}$,[21] the NTEs for the *a*- and *c*-axes are enhanced by about 49% and 117%, while the CTE for the *b*-axis is increased by only 1.9%. This explains why a ZTE is realized by the Mo:W ratio = 5:1 instead of 1:1. With increasing the contents of W, the NTEs for the *a*- and *c*-axes will be more enhanced and a linear NTE with different values is expected for the orthorhombic phase. The ZTE and variation of NCTE are attributed to the difference in electronegativity between W and Mo and the incorporation of a different amount of W, which cause variable distortion of the octahedra and softening of the MoO_4 tetrahedra, and hence an enhanced NCTE in the *a*- and *c*-axis and reduced CTE in the *b*-axis as revealed by Raman spectroscopy and XRD. The enhanced NTE result is consistent with the report about controllable thermal expansion by chemical modifications.[26]

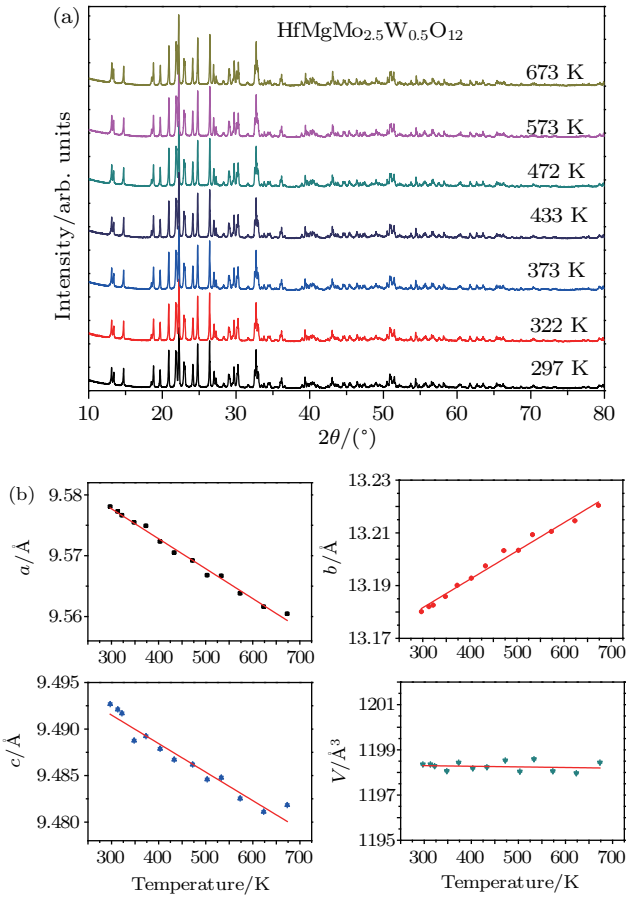


Fig. 6. (color online) (a) XRD patterns of $HfMgMo_{2.5}W_{0.5}O_{12}$ at different temperatures; (b) changes of lattice constants and volume of $HfMgMo_{2.5}W_{0.5}O_{12}$ with temperature.

4. Conclusions

$HfMgMo_{3-x}W_xO_{12}$ with $x = 0.5$, 1.0, 1.5, 1.5, 2.0, and 2.5 are synthesized by the solid solution method. Raman spectroscopic study indicates that the samples for $x \leq 2.0$ crystallize in orthorhombic structure while that for $x \leq 2.5$ adopts a monoclinic structure at RT. This is confirmed by structure refinements. A ZTE material is realized with the composition ratio of Mo:W = 5:1 and NTEs with different coefficients are obtained with increasing the contents of W. The ZTE and variation of NCTE are attributed to the difference in electronegativity between W and Mo and incorporation of a different amount of W which cause variable distortion of the octahedra and softening of the MoO_4 tetrahedra, and hence an enhanced NCTE in the *a*- and *c*-axis and reduced CTE in the *b*-axis as revealed by Raman spectroscopy and XRD.

References

[1] Mary T A, Evans J S O, Vogt T and Sleight A W 1996 *Science* **272** 90
[2] Pryde A K A, Hammonds K D, Dove M T, Heine V, Gale J D and Warren M C 1996 *J. Phys.: Condens. Matter* **8** 10973
[3] Wang Z P, Song W B, Zhao Y, Jiang Y J and Liang E J 2011 *J. Light Scatt.* **23** 250
[4] Chen J, Wang F F, Huang Q Z, Hu L, Song X P, Deng J X, Yu R B and Xing X R 2014 *Sci. Rep.* **3** 2458
[5] Yan J, Sun Y, Wang C, Chu L H, Shi Z X, Deng S H, Shi K W and Lu H Q 2014 *Scripta Mater.* **84** 19
[6] Hu L, Chen J, Fan L L, Ren Y, Rong Y C, Pan Z, Deng J X, Yu R B and Xing X R 2014 *J. Am. Chem. Soc.* **136** 13566
[7] Lama P, Das R K, Smith V J and Barbour L J 2014 *Chem. Commun.* **50** 6464
[8] Li Z Y, Song W B and Liang E J 2011 *J. Phys. Chem. C* **115** 17806
[9] Wu M M, Hu Z B, Liu Y T and Chen D F 2009 *Mater. Res. Bull.* **44** 1943
[10] Liu X S, Cheng Y G, Liang E J and Chao M J 2014 *Phys. Chem. Chem. Phys.* **16** 12848
[11] Wu M M, Peng J, Zu Y, Liu Y D, Hu Z B, Liu Y T and Chen D F 2012 *Chin. Phys. B* **21** 116102
[12] Li Q J, Yuan B H, Song W B, Liang E J and Yuan B 2012 *Chin. Phys. B* **21** 046501
[13] Bridges F, Keiber T, Juhas P, Billinge S J L, Sutton L, Wilde J and Kowach G R 2014 *Phys. Rev. Lett.* **112** 045505
[14] Wang X W, Huang Q Z, Deng J X, Yu R B, Chen J and Xing X R 2011 *Inorg. Chem.* **50** 2685
[15] Ge X H, Mao Y C, Liu X S, Cheng Y G, Yuan B H, Chao M J and Liang E J 2016 *Sci. Rep.* **6** 24832
[16] Cheng Y G, Liang Y, Ge X H, Liu X S, Yuan B H, Guo J, Chao M J and Liang E J 2016 *RSC Adv.* **6** 53657
[17] Long Y W, Hayashi N, Saito T, Azuma M, Muranaka S and Shimakawa Y 2009 *Nature* **458** 60
[18] Azuma M, Chen W, Seki H, Czapski M, Olga S, Oka K, Mizumaki M, Watanuki T, Ishimatsu N, Kawamura N, Ishiwata S, Tucker M G, Shimakawa Y and Attfield J P 2011 *Nat. Commun.* **2** 347
[19] Suzuki T and Omote A 2004 *J. Am. Ceram. Soc.* **87** 1365
[20] Gindhart A M, Lind C and Green M 2008 *J. Mater. Res.* **23** 210
[21] Marinkovic B A, Jardim P M, Ari M, Avillez R R, Rizzo1 F and Ferreira F F 2008 *Phys. Stat. Sol. (b)* **245** 2514
[22] Miller K J, Johnson M B, White M A and Marinkovic B A 2012 *Solid State Commun.* **152** 1748
[23] Lind C, Gates S D, Pedoussaut N M and Baiz T I 2010 *Materials* **3** 2567
[24] Song W B, Liang E J, Liu X S, Li Z Y, Yuan B H and Wang J Q 2013 *Chin. Phys. Lett.* **30** 126502
[25] Li F, Liu X, Song W, Yuan B, Cheng Y, Yuan H, Cheng F, Chao M and Liang E 2014 *J. Solid State Chem.* **218** 15
[26] Chen J, Hu L, Deng J X and Xing X R 2015 *Chem. Soc. Rev.* **44** 3522